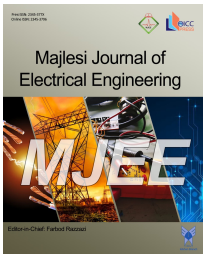

Volume 19, Issue 2, 192538 (1-15)

Majlesi Journal of Electrical Engineering (MJEE)

https://doi.org/10.57647/j.mjee.2025.1902.38

Particle swarm optimization effectiveness for selective harmonic elimination in multilevel inverters at varying output levels

Muhammad Najwan Hamidi[1,*], Dahaman Ishak[2]

[1]*School of Electrical & Electronic Engineering, University Sains Malaysia, Nibong Tebal, Malaysia.*
[2]*Electrical Engineering Department, Prince Mohammad Bin Fahd University, Al Khobar, Saudi Arabia.*

[*]**Corresponding author:** najwan@usm.my

Original Research

Received:
5 January 2025
Revised:
18 March 2025
Accepted:
9 May 2025
Published online:
1 June 2025

Abstract:

Multilevel inverters (MLI) play a pivotal role in diverse applications, notably solar power generation, owing to their capacity for generating high-quality, multiple-level output voltages with reduced total harmonic distortions (THD) in comparison to traditional inverters. Nevertheless, as MLI levels increase, challenges arise, impacting implementation feasibility due to heightened computational demands for pulse width modulation (PWM) generation. Researchers have inclined towards low-frequency, pre-calculated switching signal methods, although these tend to induce higher output harmonics, particularly at lower levels. This study focuses on studying the significance of employing the particle swarm optimization (PSO) technique to solve selective harmonic elimination (SHE) equations (SHE-PSO) in MLI applications, evaluating its impact on THD at various output levels (3L, 5L, and 7L) within a cascaded H-bridge MLI. Results are compared with simpler methods, namely sine-based calculation (SBC) and Newton Raphson-based SHE (SHE-NR). The findings illustrate that SHE-PSO effectively minimizes lower-order harmonics to as low as 0%, outperforming SBC and NR. However, in terms of THD, SHE-PSO proves advantageous only at 5L, with SHE-NR exhibiting superior performance at other levels. This study concludes that the reduction of lower-order harmonics in MLI does not necessarily translate to an overall improvement in THD, particularly at higher levels.

Keywords: Multilevel inverter; Particle swarm optimization; Low-order harmonics; Total harmonic distortion; Selective harmonic elimination

1. Introduction

Inverters, in general, are used to transform the voltage from direct current (DC) to alternating current (AC). Inverters are one of the most important parts in almost all electrical power systems where they have been utilized in various sectors including solar power generation and electric vehicle industries [1]. Multilevel inverter (MLI) is a more recently introduced family of inverters which are built from the assembly of power semiconductors, voltage sources and other components, which jointly generate voltages recognized by their stepped waveforms. MLIs have gained substantial prominence as a feasible solution to overcome the limitations posed by traditional two-level inverters. MLI showcase the capability to produce higher-quality, multiple-levelled output voltage while posing the capability to effectively minimize the existence of harmonic distortions [2]. This feature contributes to the reduced need for huge filtering at the output. MLI are also notable in their suitability to operate in multiple high-power applications as compared to traditional inverters. Additionally, due to the nature of their outputs, MLIs are also suited to be operated using lower switching frequency modulation, resulting in decreased switching losses and prolonged durability of the system [3].

Throughout the years, there has been a consistent increase in the number of MLI topologies published in the literature at which each one of them would introduce additional advantages. One thing to note is that almost all of the proposed MLI topologies are usually designed to be modular and easily scalable. Thus, a topology is able to produce any number of output levels as required by designers by extending the circuit configuration. The rule of thumb in MLI is that as the number of levels is increased, the total harmonic distortion (THD) will decrease, at the cost of a higher

number of components requirement [4, 5]. Challenges in implementation come as the number of levels is increased. When the traditional pulse width modulation (PWM)-based, high-switching frequency (HSF) techniques are used, the number of carrier signals required will also increase according to the increase in level. The number of carrier signals required could be very high, which reduces the feasibility of such a system being implemented for real applications due to the high processing power requirement [6]. For instance, one study [7] reported that a 7-level inverter required six carrier signals for switching pulse generation, while another study [8] demonstrated that a 9-level inverter required eight carrier signals. Generally, the number of carrier signals needed is approximately equal to the number of levels (N_L) minus one ($N_L - 1$). Recent research efforts have focused on reducing the number of required carrier signals. However, the number remains relatively high, especially as the number of levels increases. For example, a modified modulation technique was shown to require 11 carrier signals for generating 19 output levels [9], highlighting the ongoing challenge of balancing complexity and efficiency in MLI systems.

Thus, at a higher number of levels, researchers have been implementing low switching frequency modulation (LSF) techniques to reduce the burden on microcontrollers. One of the most basic methods for LSF modulation is the equal phase method where the angles for the switching signals are pre-calculated [10]. However, this method distributes the switching angles equally based on the number of output levels. So, the output waveforms appear slightly triangular in shape with a considerably high value of THD [11]. Extending from this idea, another switching angles calculation method dubbed the sine-based calculation (SBC) method is introduced where the idea is based on the fact that a pure sinusoidal waveform is wider in shape in the middle of every half-cycle and narrower at the beginning and end of the two half-cycles [12]. Using this method, the output levels of MLI will be in closer resemblance to a pure sine wave, reducing the THD. The nearest level control (NLC) technique has also been demonstrated to produce similar switching signals to the SBC despite producing them in a slightly different manner [13]. However, it is best to note that these types of pre-calculation methods tend to produce high lower-order harmonics components. The selective harmonic elimination technique (SHE) is another LSF modulation method which is widely used. Designers are able to selectively remove any lower-order harmonics using his method. However, since non-linear transcendental equations are used for the switching angle calculation, the complexity of solving the equations is high [14, 15]. The number of equations increases with the number of levels. By using computational methods with the like of metaheuristic algorithms, the calculation can be made easier, but could also require greater computational power [16]. Among these, particle swarm optimization (PSO) has emerged as a reliable approach for solving SHE equations, enabling the determination of optimized switching angles and achieving superior harmonic reduction [17].

Both HSF and LSF have their own advantages and disadvantages. Generally, there is a trade-off between the switching frequency and output harmonics. Lower switching losses can be expected when LSF is used, but the THD is possibly higher when the number of output levels is low. But, the conduction losses will be higher [13, 18]. If the output doesn't meet the required standards for its intended use, filters are very commonly necessary. However, since MLI with a high number of output levels already produces a very low THD, the adverse effect of the high harmonics is overcome and this can subsequently eliminate the requirement for passive filtering [19]. On the other hand, the HSF technique will have lower conduction and higher switching losses.

The literature review reveals a significant gap in research concerning the implementation of advanced optimization techniques for calculating switching angles, specifically in MLI systems, and their implications or limitations when applied to MLIs with a high number of output levels. Previous studies have primarily focused on the implementation methods and simplification of solutions for simultaneous equations. However, there is a scarcity of research investigating the importance or advantages of these optimizations for MLI systems.

When implementing the SHE LSF modulation technique with any metaheuristic algorithm with the like of PSO for computation, optimized switching angles can be obtained. However, there is a lack of studies conducted on the significance of using such a method towards the THD of the system when MLI is considered. The motivation of this research is to investigate the viability of incorporating advanced optimization techniques for calculating switching angles in MLI systems. The aim is to determine whether optimizing switching angles offers significant benefits, particularly at higher numbers of MLI levels, given that the primary objective of MLI introduction is already to mitigate harmonics. Through this investigation, researchers aim to ascertain whether switching angle optimization contributes positively to the final design in terms of harmonic performance, processing power, and potential additional costs, such as those associated with enhanced microcontroller requirements.

In this paper, the significance of the PSO optimization technique is thoroughly studied for MLI applications at different number of levels. This study is conducted to explore whether such a method is able to produce better outputs at different numbers of output levels as compared to the much simpler pre-calculated methods in terms of individual harmonic contents and THD. All computations are done using MATLAB and simulations are conducted using Simulink.

2. Model description

2.1 Cascaded H-Bridge MLI

Since circuit topology is not related to the MLI output levels production, in this paper, the cascaded H-Bridge (CHB) MLI inverter is implemented for its ease of implementation. The generalized figure of the CHB topology is depicted in Fig. 1. In this work, the circuit is tested at three distinct numbers of output levels: 3 levels (3L), 5 levels (5L) and 7 levels (7L). The number of DC sources and H-Bridge units required to generate the 3L, 5L and 7L outputs are 1, 2 and

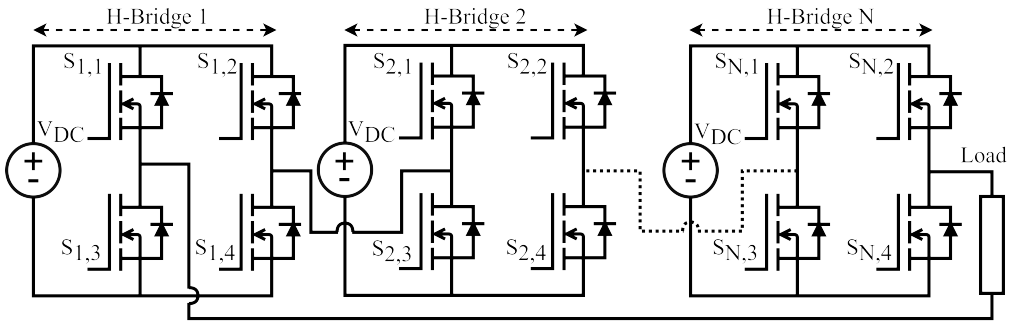

Figure 1. General structure of CHB MLI topology.

3, respectively. Additionally, a symmetrical voltage source configuration is used where all the implemented DC sources will share the same magnitude. The general switching table for a CHB MLI topology is given in Table 1.

2.2 SBC method

The first switching method implemented in this work is the SBC method where the switching angles are pre-calculated using mathematical equations, in relation to a pure sinusoidal waveform. The calculated angle values can then be loaded into a microcontroller in the form of a look-up table. Thus, only minimal processing power would be required since there is no active modulation operation being carried out. However, in this study, only simulation-based work is considered. Therefore, the calculated switching angles are directly used in the MATLAB/Simulink simulation for generating the switching pulses. For any number of levels, the calculation can be separated into four different segments for ease of understanding as shown in Fig. 2 (a). The first segment is from the start of the waveform until the midpoint of the positive half-cyle. The second segment is from the midpoint up to the end of the positive half-cycle. Similarly, the third and the fourth segments are from the start until the midpoint of the negative half-cycle and from the midpoint until the end of the waveform, respectively. For the calculation of the switching angles in the first portion, the following equation is used

$$\theta_P = \sin^{-1}\left[\frac{1}{M(N_L-1)(2P-1)}\right] \text{ for } P = 1,2,\ldots,\frac{N_L-1}{2} \tag{1}$$

where N_L is the number of output levels produced by the CHB MLI, M is the modulation index and θ_P is the switching angles during the positive half-cycle which is from 0° up to N_L-1. Then, the switching angles for the second segment can be calculated as given in (2). Note that, exactly at the end of the first half-cycle or at the start of the second half-cycle, the angle is 180° as given in (3).

$$\theta_P = 180 - \sin^{-1}\left[\frac{1}{M(N_L-1)(2P-1)}\right] \text{ for } P = \frac{N_L-1}{2},\ldots,2,1 \tag{2}$$

$$\theta_P = 180 \text{ for } P = N_L \tag{3}$$

Lastly, since the output waveform at the positive and negative half-cycles should have a similar shape except for the inverted polarity, the switching angles for the third and fourth segments can be easily calculated as follows

$$\theta_N = 360 - \theta_P \text{ for } N = N_L-1,\ldots,2, \tag{4}$$

Table 1. General switching table of CHB MLI topology.

ON Switches				Output voltage
H-Bridge 1	H-Bridge 2	...	H-Bridge N	
$S_{1,1}$, $S_{1,2}$	$S_{2,1}$, $S_{2,2}$	...	$S_{N,1}$, $S_{N,2}$	0
$S_{1,1}$, $S_{1,4}$	$S_{2,1}$, $S_{2,2}$	...	$S_{N,1}$, $S_{N,2}$	V_{DC}
$S_{1,1}$, $S_{1,4}$	$S_{2,1}$, $S_{2,4}$	...	$S_{N,1}$, $S_{N,2}$	$2\times V_{DC}$
⋮	⋮	⋮	⋮	⋮
$S_{1,1}$, $S_{1,4}$	$S_{2,1}$, $S_{2,4}$	...	$S_{N,1}$, $S_{N,4}$	$N\times V_{DC}$
$S_{1,2}$, $S_{1,3}$	$S_{2,2}$, $S_{2,3}$	...	$S_{N,2}$, $S_{N,3}$	$-N\times V_{DC}$
⋮	⋮	⋮	⋮	⋮
$S_{1,2}$, $S_{1,2}$	$S_{2,2}$, $S_{2,3}$	...	$S_{N,3}$, $S_{N,4}$	$-2\times V_{DC}$
$S_{1,2}$, $S_{1,2}$	$S_{2,3}$, $S_{2,4}$	...	$S_{N,3}$, $S_{N,4}$	$-V_{DC}$
$S_{1,3}$, $S_{1,4}$	$S_{2,3}$, $S_{2,4}$	...	$S_{N,3}$, $S_{N,4}$	0

where θ_N are the switching angles during the negative half-cycle which is from 180° up to $2N_L - 1$. Each calculated switching angle represents the start point of each output level. For the three output level settings, the positionings of the calculated switching angles using the SBC method are depicted in Fig. 2 (b) to Fig. 2 (d). The total number of switching signals at any output level is equal to $2N_L$. For the three tested output levels, the calculated switching angles are presented in section 3.

2.3 SHE-PSO method

The second switching method to be analysed in this work is the SHE-PSO method where the SHE equations are solved using PSO which is a metaheuristic optimization algorithm. Using this method, certain lower-order harmonics can be minimised or totally eliminated through proper calculation of the switching angles. To utilize the SHE technique, it is necessary to formulate Fourier series expansions of the periodic output waveform generated by the MLI. Typically, this Fourier extension can be expressed as follows

$$f(x) = \frac{1}{2}a_0 + \sum_{n=1}^{\infty} a_n \cos(nx) + \sum_{n=1}^{\infty} b_n \sin(nx) \tag{5}$$

It is best to note that the output voltage of an inverter is generally a sinusoidal waveform. Due to the fact that a sinusoidal waveform is an odd and quarter-wave symmetry which is when the waveform is symmetric about the origin and satisfies the $f(-t) = -f(t)$ condition, thus a_0 and a_n is equal to 0. Under this case, the switching angles calculation can be reduced down to only the midpoint of the overall signal which is at $\pi/2$. Using the quarter-wave symmetry rule, the other switching signals can easily be calculated. Thus, the Fourier extension of the output voltage of an inverter can be reduced down to

$$V_0(\omega t) = \sum_{n=1}^{\infty} V_n \sin(n\omega t) \tag{6}$$

where V_n is the voltage magnitude at a specific harmonic order. To calculate V_n for the 5L, 7L and 9L MLI, the Fourier expression V_n of equations (7), (8) and (9) can be used, respectively

$$\begin{cases} V_1 = \frac{4V_{DC}}{\pi}[\cos(\theta_1) + \cos(\theta_2)] \\ V_3 = \frac{4V_{DC}}{3\pi}[\cos(3\theta_1) + \cos(3\theta_2)] \\ V_5 = \frac{4V_{DC}}{5\pi}[\cos(5\theta_1) + \cos(5\theta_2)] \end{cases} \tag{7}$$

$$\begin{cases} V_1 = \frac{4V_{DC}}{\pi}[\cos(\theta_1) + \cos(\theta_2) + \cos(\theta_3)] \\ V_3 = \frac{4V_{DC}}{3\pi}[\cos(3\theta_1) + \cos(3\theta_2) + \cos(3\theta_3)] \\ V_5 = \frac{4V_{DC}}{5\pi}[\cos(5\theta_1) + \cos(5\theta_2) + \cos(5\theta_3)] \\ V_7 = \frac{4V_{DC}}{7\pi}[\cos(7\theta_1) + \cos(7\theta_2) + \cos(7\theta_3)] \end{cases} \tag{8}$$

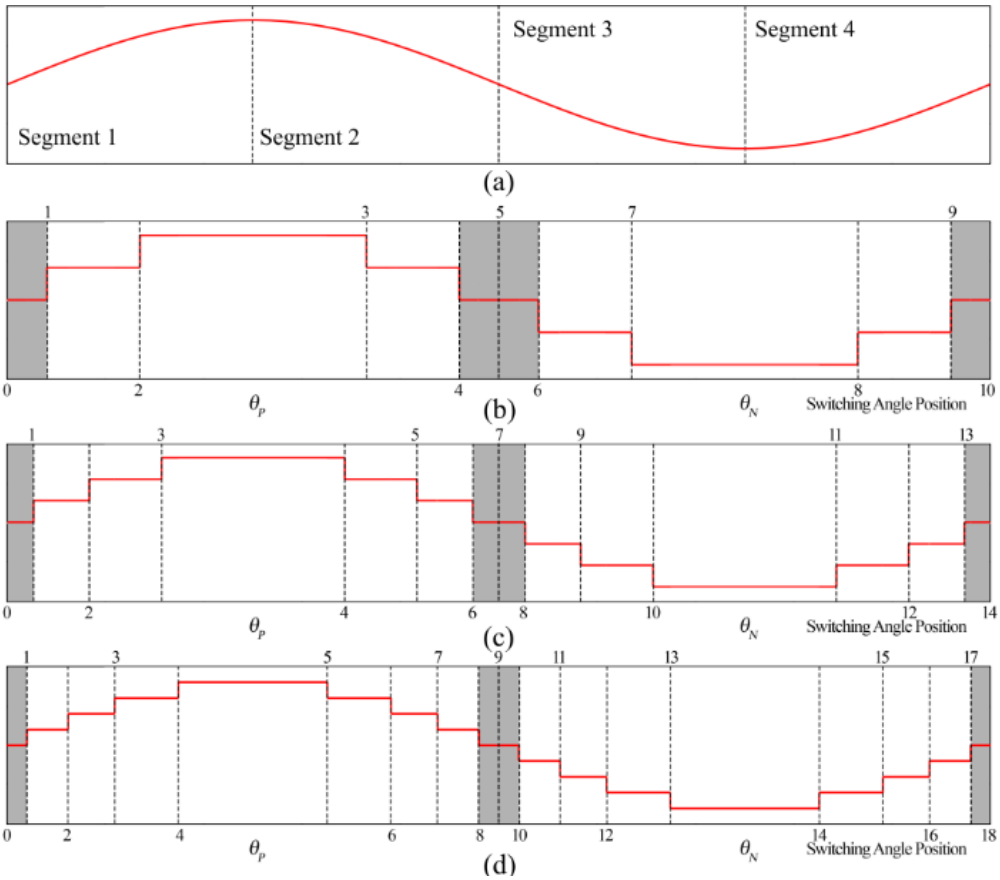

Figure 2. Depiction of (a) the four switching segments relative to a pure sinusoid. (b) 5L switching positions. (c) 7L switching positions. (d) 9L switching positions.

$$\begin{cases} V_1 = \frac{4V_{DC}}{\pi}[\cos(\theta_1)+\cos(\theta_2)+\cos(\theta_3)+\cos(\theta_4)] \\ V_3 = \frac{4V_{DC}}{3\pi}[\cos(3\theta_1)+\cos(3\theta_2)+\cos(3\theta_3)+\cos(3\theta_4)] \\ V_5 = \frac{4V_{DC}}{5\pi}[\cos(5\theta_1)+\cos(5\theta_2)+\cos(5\theta_3)+\cos(5\theta_4)] \\ V_7 = \frac{4V_{DC}}{7\pi}[\cos(7\theta_1)+\cos(7\theta_2)+\cos(7\theta_3)+\cos(7\theta_4)] \\ V_9 = \frac{4V_{DC}}{9\pi}[\cos(9\theta_1)+\cos(9\theta_2)+\cos(9\theta_3)+\cos(9\theta_4)] \end{cases} \tag{9}$$

where V_{DC} is the voltage source magnitude, n is the harmonic order and θ_n is the switching angle. From the expressions, it can be concluded that the number of switching signals to be calculated is equal to $(N_L-1)/2$ which is also the number of lower order odd harmonics that are targetted to be minimised. For instance, only the 3rd and 5th harmonics will be able to be minimised for the $5L$ inverter and two switching angles will need to be calculated to achieve it. The modulation index (M) of the switching technique is related to the following equation

$$M = \frac{\pi V_1}{4V_{DC}} \tag{10}$$

To ensure proper generation of output MLI output waveform without any missing levels, the following condition needs to be met

$$0 < \theta_1 < \theta_3 < \ldots < \theta_n < \frac{\pi}{2} \tag{11}$$

With condition (11), every subsequent switching angle will have a larger value than the previous angle and a smaller value than the next angle. From all the SHE equations presented, the PSO optimisation algorithm can then be implemented. The aim of the PSO algorithm is to minimise the THD of the output waveform by minimising the selected individual harmonics as previously mentioned. The technique is based on the social behavior of swarms searching for food. The PSO algorithm is initialised with a swarm of particles each of which has a random position and speed. In an effort to locate the optimum solution, the particles wander across the problem's search space. Based on its own prior experiences as well as the prior experiences of other particles in the swarm, each particle modifies its position and velocity. Based on their local and global best solutions, the particles' velocities and locations are updated. This facilitates the particles' gradual movement towards better solutions and lastly, the best solution. The PSO equations used to update the position (x) and velocity (v) of the particles are given as follows

$$x_i^{t+1} = x_i^t + v_i^{t+1} \tag{12}$$

$$v_i^{t+1} = w \cdot v_i^{t+1} + c_1 U_1^t (Pb_1^t - x_i^t) + c_2 U_2^t (g_b^t - x_i^t) \tag{13}$$

where x_i is the i^{th} particle position, v_i is the i^{th} particle velocity, c_1 and c_2 are positive valued acceleration constants, U_1 and U_2 are random variables between the value of 0, w is the inertia weight, P_b is the best position found by a particle at the current iteration and g_b is the best position found by any particle in the swarm at the current iteration. The iteration is represented by t where t is the current iteration and $t+1$ is the next iteration. The basic flowchart of PSO algorithm operation is given in Fig. 3. For the lower order

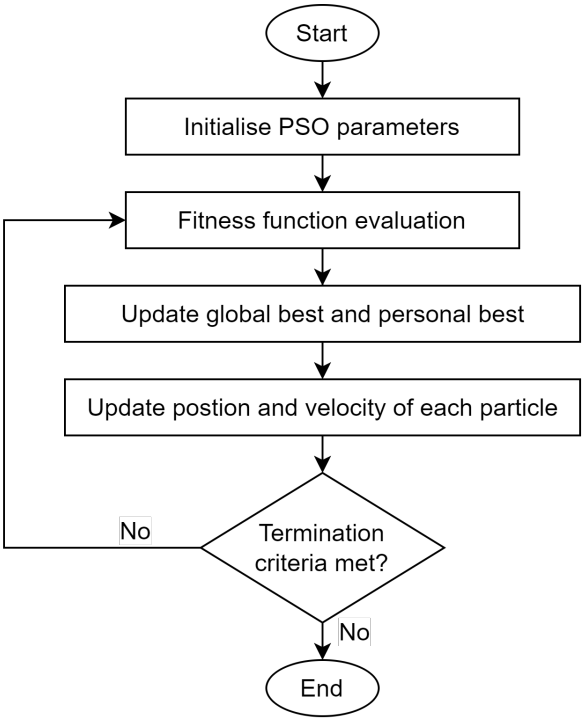

Figure 3. PSO algorithm.

harmonics elimination using the PSO algorithm, the THD equation is implemented as the fitness function as given

$$\text{THD} = \frac{\sqrt{\sum_{n=1(\text{odd})}^{N_L} V_n^2}}{v_1} \tag{14}$$

To further improve the performance of the PSO algorithm, the damping ratio is considered in the algorithm. It is based on the method proposed in [20]. With the damping ratio parameter, the particle velocities are reduced over time which will help prevent the PSO algorithm from being stuck in local minima. Apart from that, the convergence rate of the algorithm is also expected to be improved. All the parameters selected for the PSO algorithm in this work are tabulated in Table 2. Unlike the SBC method, which determines switching angles through analytical calculations, the SHE-PSO technique is a heuristic algorithm that relies on stochastic processes to approximate near-optimal solutions. Although it does not guarantee an exact optimal solution, it can achieve results very close to optimal while significantly reducing the complexity of analytical computations. The switching angles are determined using MATLAB code

Table 2. Selected PSO parameters.

Parameters	Values
Maximum iteration	1000
Number of population (Swarm size)	100
Inertia weight (w)	1
Damping ratio (d)	0.99
Constant (C_1)	2
Constant (C_2)	2
Variable lower bound	0
Variable upper bound	$\pi/2$

based on the SHE-PSO method. Once obtained, these angles are applied in Simulink in a similar manner to the SBC method, with the only difference being the use of a different set of angles.

2.4 Assumptions

Based on the presented model descriptions, several assumptions have been made which are supported both by objective reasoning as well as through literature review. These assumptions are listed as follows.

- Assumption 1: The MLI topology does not influence the characteristics of the output waveforms; instead, these waveforms are solely determined by the switching pattern. For example, the output waveform of a 9-level MLI generated by a cascaded H-Bridge inverter exhibits similar characteristics to that of another 9-level MLI topology when both employ the same switching pattern.
- Assumption 2: Switching can be accomplished with minimal processing power when employing precalculated switching angles, as opposed to active modulation, where switching angles are loaded directly onto the microcontroller without requiring any active modulation operations within it.
- Assumption 3: The voltage outputs generated by an MLI exhibit a symmetrical waveform characterized by odd and quarter-wave symmetry, where the waveform is mirrored across the origin. This characteristic assumption forms the basis for formulating equations in the SBC method.

2.5 Simulation model

Based on the presented model descriptions, several assumptions have been made which are supported both by logical thinking as well as *t*.

3. Results and discussion

In the first part of the analysis, all the switching angles are calculated using the SBC and SHE-PSO methods. Additionally, for additional comparison, switching angles calculated using SHE-Newton Raphson (SHE-NR) found from literature are also included [21–23]. The implementation of the SHE-NR method follows a similar approach to the SBC and SHE-PSO methods in Simulink. The calculated switching angles using the three methods for the three tested MLI levels are tabulated in Table 3, Table 4, and Table 5. An evident observation appears from the examination of Table 3, Table 4, and Table 5, revealing that the switching angles obtained through the three methods exhibit notable dissimilarities.

From the calculated switching signals, MATLAB/Simulink software is used to simulate the MLI circuits. In this study, the output voltage is set to 230 Vrms (325.27 Vpeak) at the frequency of 50 Hz. To achieve this peak value, the magnitude selection of the DC sources will need to follow the following relationship.

$$V_{DC} = \frac{230\sqrt{2}}{N_{DC}} \tag{15}$$

Table 3. Calculated switching angles for the 5L MLI.

Switching position	Switching Angle (°)		
	SBC	SHE-PSO	SHE-NR [21]
θ_1	14.478	12.000	14.7361
θ_2	48.590	48.000	50.7361

Table 4. Calculated switching angles for the 7L MLI.

Switching position	Switching Angle (°)		
	SBC	SHE-PSO	SHE-NR [21]
θ_1	9.594	11.671	11.68
θ_2	30.000	26.936	31.18
θ_3	56.443	56.056	58.58

Table 5. Calculated switching angles for the 9L MLI.

Switching position	Switching Angle (°)		
	SBC	SHE-PSO	SHE-NR [21]
θ_1	7.181	0.857	7.5
θ_2	22.024	24.857	21.6
θ_3	38.682	35.143	36.8
θ_4	61.045	60.860	60.2

where N_{DC} is the number of DC sources. From equation (15), the N_{DC} values for the 5L, 7L and 9L MLI are calculated to be 162.63 V, 108.42 V and 81.32 V, respectively. These values ensure that the inverter's output voltage equals 230 Vrms. For example, in the case of the 5L inverter, where $N_{DC} = 2$, the output peak voltage is 162.63 V + 162.63 V = 325.26 Vpeak, corresponding to 230 Vrms. The circuit, as depicted in figure 1, is modelled in Simulink based on the number of levels, where the number of H-Bridge modules corresponds to 2, 3, and 4 for the 5L, 7L, and 9L outputs, respectively. To implement the calculated switching angles, the "Stair Generator" block is employed to generate the required switching pulses. Specifically, the "Stair Generator" can operate using a lookup table to achieve the desired pulse generation.

The MLI topologies are first tested under a purely resistive (R) load value of 52.9 Ω (1 kW). The harmonic contents of the output voltage and current for the 5L, 7L and 9L MLI are presented in Table 6 and Table 7. In Simulink, the individual harmonic components are analyzed using Fast Fourier Transform (FFT). Measurements are taken only after the inverters reach steady-state operation, with data collected over 5 cycles. The simulation duration for all tested systems is set to 1 s, with a sample time of 1 μs, ensuring that the last five cycles used for harmonic computation are well within the steady-state operation. From the results obtained under all three types of MLIs, the voltage and current share

Table 6. MLI output voltage harmonic content with $R = 52.9\ \Omega$.

	Voltage Harmonic Content (V)								
	5L			7L			9L		
Order	SBC	SHE-PSO	SHE-NR	SBC	SHE-PSO	SHE-NR	SBC	SHE-PSO	SHE-NR
1st	335 (100%)	338.7 (100%)	330.1 (100%)	328.5 (100%)	331.8 (100%)	333.1 (100%)	325 (100%)	327.9 (100%)	328.6 (100%)
3rd	6.73 (2.01%)	0.20 (0.06%)	11.42 (3.46%)	4.53 (1.38%)	0.27 (0.08%)	0.30 (0.09%)	3.09 (0.95%)	0.39 (0.12%)	0.43 (0.13%)
5th	6.20 (1.85%)	0.07 (0.02%)	0.03 (0.01%)	0.43 (0.13%)	0.03 (0.01%)	0.07 (0.02%)	1.50 (0.46%)	0.10 (0.03%)	0.10 (0.03%)
7th				6.60 (2.01%)	0.07 (0.02%)	7.93 (2.38%)	2.05 (0.63%)	0.03 (0.01%)	0.07 (0.02%)
9th							5.95 (1.83%)	0.10 (0.03%)	7.98 (2.43%)

Table 7. MLI output current harmonic content with $R = 52.9\ \Omega$.

	Current Harmonic Content (A)								
	5L			7L			9L		
Order	SBC	SHE-PSO	SHE-NR	SBC	SHE-PSO	SHE-NR	SBC	SHE-PSO	SHE-NR
1st	6.333 (100%)	6.403 (100%)	6.24 (100%)	6.21 (100%)	6.272 (100%)	6.297 (100%)	6.144 (100%)	6.198 (100%)	6.212 (100%)
3rd	0.1273 (2.01%)	0.0038 (0.06%)	0.2159 (3.46%)	0.0857 (1.38%)	0.0050 (0.08%)	0.0057 (0.09%)	0.0584 (0.95%)	0.0074 (0.12%)	0.0081 (0.13%)
5th	0.1172 (1.85%)	0.0013 (0.02%)	0.0006 (0.01%)	0.0081 (0.13%)	0.0006 (0.01%)	0.0013 (0.02%)	0.0283 (0.46%)	0.0019 (0.03%)	0.0019 (0.03%)
7th				0.1248 (2.01%)	0.0013 (0.02%)	0.1499 (2.38%)	0.0387 (0.63%)	0.0006 (0.01%)	0.0012 (0.02%)
9th							0.1124 (1.83%)	0.0019 (0.03%)	0.1510 (2.43%)

similar percentages of harmonic content when powering a purely *R* load.

For the 5L MLI, at the fundamental harmonic order, it is evident that all approaches exhibit comparable performance, displaying slight variations in voltage and current harmonic values. However, at the 3rd harmonic order, SHE-NR demonstrates notably higher voltage and current harmonics compared to SBC and SHE-PSO. Moving to the 5th harmonic order, both voltage and current harmonics are minimized for SHE-NR, whereas SHE-PSO exhibits slightly higher harmonics. Overall, among the three techniques, the SHE-PSO method appears to have effectively minimized lower-order harmonic contents. Despite the fact that the SHE-NR method is designed to reduce lower-order harmonics, it produces the highest magnitudes at specific harmonic orders which are observable at the 3rd harmonic for the 5L inverter, the 7th harmonic for the 7L, and the 9th harmonic for the 9L. This occurs because the NR method requires an excellent initial guess to converge to the optimal solution. Without a good initial guess, the method may either diverge or converge to a local minimum. Moreover, the nonlinear and transcendental nature of the SHE equations poses additional challenges for *NR*, particularly as the number of variables increases, further complicating convergence. In contrast, the SHE-PSO method consistently demonstrates an effective reduction of lower-order harmonics across all tested conditions. This is attributed to its fundamentally different approach to solving the SHE equations. As a stochastic optimization technique, PSO explores the global solution space, effectively avoiding local minima. Additionally, it does not rely on derivatives, enabling it to handle nonlinearities more efficiently. Fig. 4 depicts the 5L output waveforms produced by the three methods, while Fig. 5 provides close-up views of each level transitioning states, highlighting variations in switching angles.

In the case of the 7L inverter, at the 1st Harmonic Order, all three systems exhibit similar voltage and current harmonic values, with slight variations. At the 3rd harmonic order, SBC shows significantly higher harmonics compared to SHE-PSO and SHE-NR. However, the harmonic content

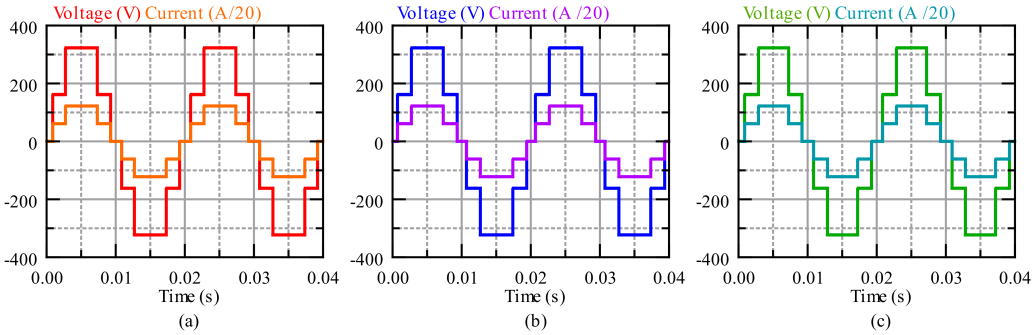

Figure 4. 5L output waveforms with $R = 52.9\ \Omega$ generated by (a) SBC. (b) SHE-PSO. (c) SHE-NR.

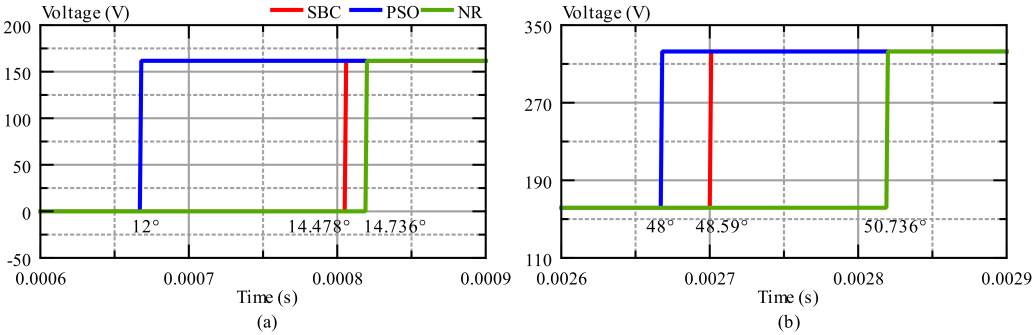

Figure 5. 5L MLI output level transition point for the change from (a) 0 to V_{DC}. (b) V_{DC} to $2V_{DC}$.

is considerably low and relatively similar in SHE-PSO and SHE-NR. Moving to the 5th harmonic order, once again, SBC exhibits higher harmonics, while both SHE-PSO and SHE-NR maintain relatively similar and reduced values. Finally, at the 7th harmonic order, a drastic increase in harmonics is observed in SHE-NR, while SHE-PSO remains at a low and reduced level. Similar to the 5L MLI, the PSO-SHE successfully minimizes the lower-order harmonic content compared to the other techniques. Fig. 6 displays the output waveforms for the 5L configuration generated by three methods, while Fig. 7 offers detailed views of individual levels transitioning states, emphasizing differences in switching angles.

As for the 9L MLI, at the 1st harmonic order, the voltage

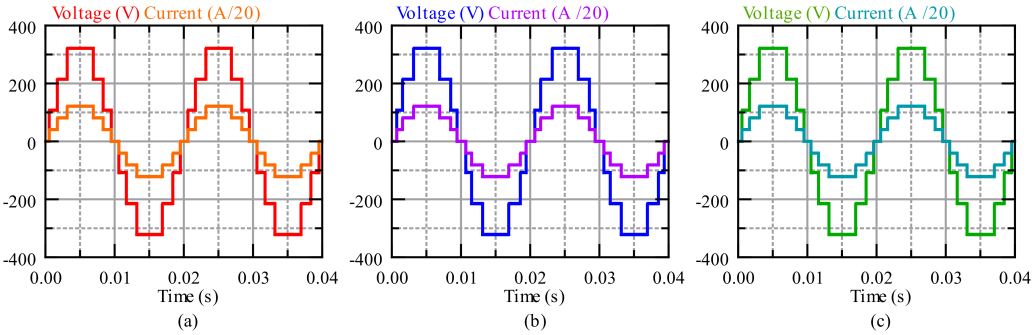

Figure 6. 7L output waveforms with $R = 52.9\ \Omega$ generated by (a) SBC. (b) SHE-PSO. (c) SHE-NR.

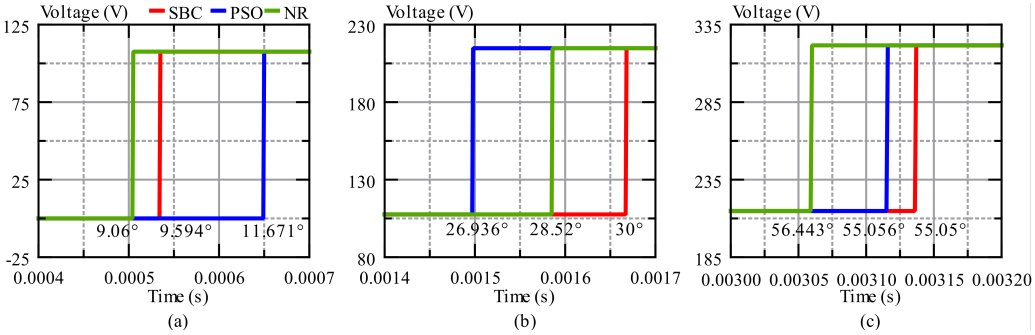

Figure 7. 7L MLI output level transition point for the change from (a) 0 to V_{DC}. (b) V_{DC} to $2V_{DC}$. (c) $2V_{DC}$ to $3V_{DC}$.

and current levels are relatively comparable among the three techniques. Similar to the 7L MLI, at the 3rd harmonic order, SHE-PSO and SHE-NR exhibit significantly reduced harmonic contents with very similar values. This trend persists at the 5th harmonic order, where the harmonic contents produced by SHE-PSO and SHE-NR are further reduced with very similar values. Moving to the 7th harmonic order, the trend continues for SHE-PSO, while the harmonic content of SHE-NR significantly increases. Overall, it is evident that SHE-PSO is highly effective in minimizing lower-order harmonics, whereas SHE-NR can only effectively minimize certain lower-order harmonics. Fig. 8 shows the 5L output waveforms generated by the three methods, and Fig. 9 presents detailed views of each level as it changes states, emphasizing differences in switching angles.

In Simulink, the computation of THD is also performed using different computational methods that exist for determining THD, depending on the maximum frequency considered. To obtain the overall THD, the Nyquist frequency is commonly employed in the calculation. This approach provides a close approximation of the true THD value. Fig 10 and Table 8 display the voltage THD values obtained through the three techniques computed at various maximum harmonic orders under the tested purely R load. When the maximum harmonic order for computation is set at NL, it is evident that the SHE-PSO technique produces outputs with significantly lower THD, demonstrating its effectiveness in eliminating lower-order harmonics. Since the computation is confined to NL, a reduction in lower-order harmonics directly translates to a reduction in THD. Consequently, under all tested conditions, SHE-PSO achieves the lowest THD values when computation is limited to NL. This indicates that for 5L, 7L, and 9L inverters, the THD calculations are confined to the 5th, 7th, and 9th harmonic orders, respectively.

In this study, the maximum harmonic orders selected for

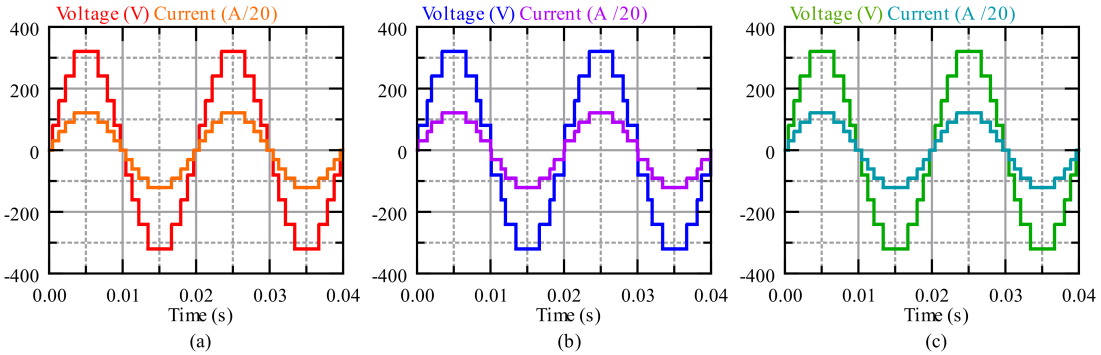

Figure 8. 9L output waveforms with $R = 52.9\ \Omega$ generated by (a) SBC. (b) SHE-PSO. (c) SHE-NR.

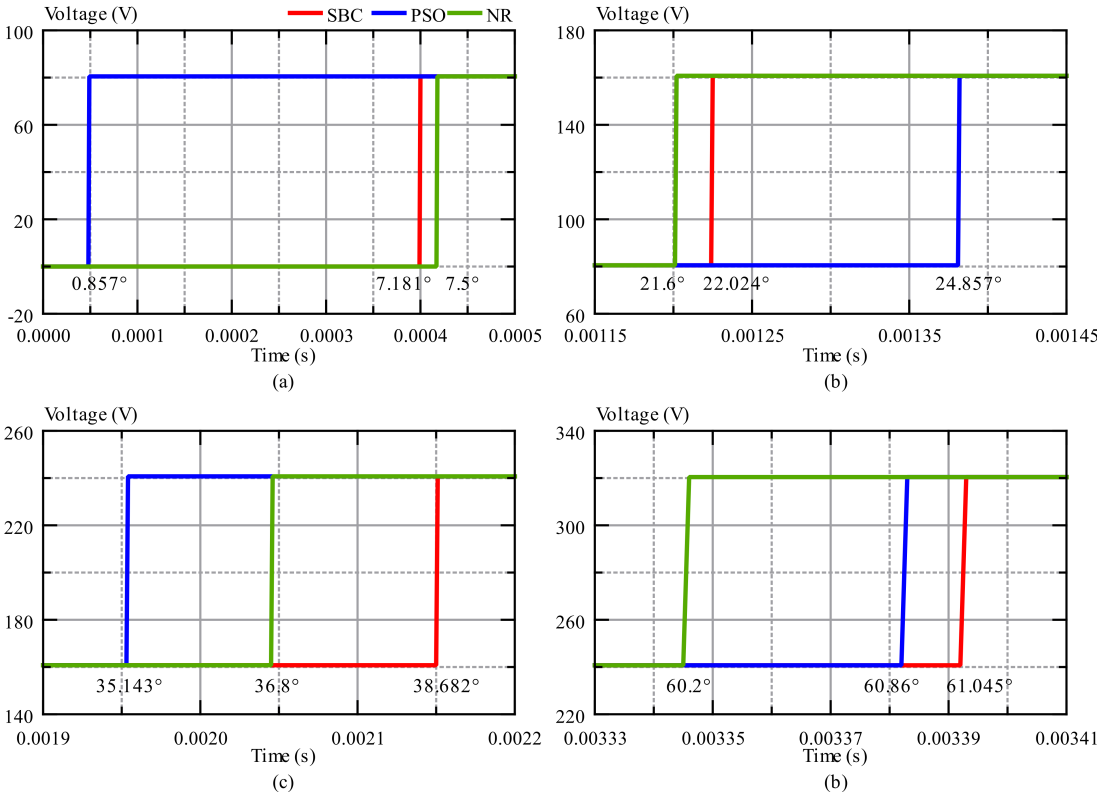

Figure 9. 9L MLI output level transition point for the change from (a) 0 to V_{DC}. (b) V_{DC} to $2V_{DC}$. (c) $2V_{DC}$ to $3V_{DC}$. (d) $3V_{DC}$ to $4V_{DC}$.

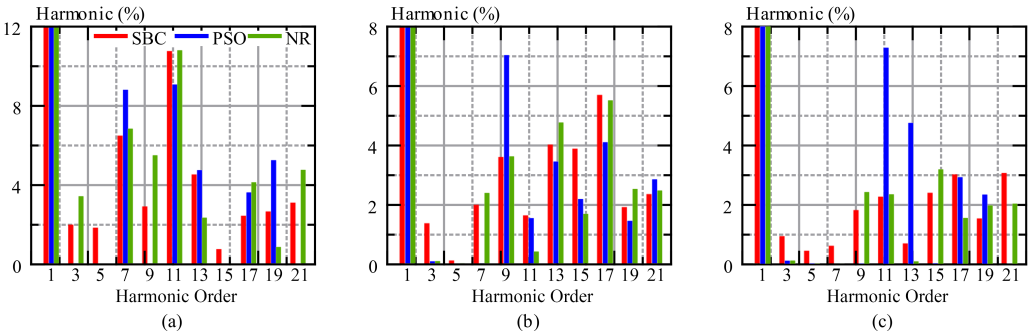

Figure 10. MLI output voltage and current harmonics with $R = 52.9\ \Omega$ at (a) 5L. (b) 7L. (c) 9L.

THD computation are 39, 49, 59, and the Nyquist frequency. These values are chosen to align with and demonstrate compliance with various international standards. For example, according to the IEC 61000-3-2 standard, THD calculations are performed up to the 40th harmonic order. Since only odd-order harmonics are present in this study, the 39th harmonic order is selected as the upper limit. In contrast, the IEEE 519-2022 standard recommends analyzing harmonics up to at least the 50th order for most practical applications. This ensures a more comprehensive assessment of THD across a broader spectrum of harmonics, reflecting real-world conditions more accurately.

For example, in the case of the 5L MLI, SHE-PSO exhibits the lowest overall THD, followed by SBC and SHE-NR. However, the difference between SHE-PSO and SBC is not significant. In contrast, for the 7L and 9L MLIs, SHE-NR actually achieves the lowest THDs, while SHE-PSO has the highest THDs. Consequently, it can be concluded that, for MLIs, effectively reducing the overall THD is more challenging as the number of levels increases. The need to eliminate lower-order harmonics becomes less significant in terms of reducing the overall THD as the number of levels rises. The current THDs are exactly similar to the voltage THDs as presented in Table 8 under the purely *R* load tests. While lower-order harmonics typically have higher magnitudes and contribute significantly to the THD, minimizing them does not necessarily guarantee a reduction in THD. This is because THD is a comprehensive measure of the total distortion in the waveform, encompassing the cumulative impact of all harmonics relative to the fundamental frequency. If the higher-order harmonics remain significant, the overall THD can still remain high. Additionally, minimizing lower-order harmonics may lead to spectrum redistribution, where the distortion shifts to higher-order components. This redistribution can result in an increase in THD, as the remaining distortion may not be uniformly reduced across the harmonic spectrum. Table 8 illustrates this phenomenon, showing variations in THD values at different maximum harmonic orders considered in the computations. These variations highlight how higher-order harmonics can still exhibit considerable magnitudes, significantly influencing the overall THD. The most accurate THD values are those computed up to the Nyquist frequency, as this approach captures the complete harmonic spectrum within the system's bandwidth, providing a more comprehensive assessment of waveform distortion.

Next, the MLI configurations undergo additional testing with a resistive-inductive (*RL*) load having a value of 36 Ω − 0.153 H (approximately 880 kVA at a power factor of 0.6). The harmonic profiles of the output voltage and current for the 5L, 7L, and 9L MLI setups are outlined in Table 9 and Table 10. The *RL* component functions as a low-pass filter, resulting in observable reductions in the values of output current harmonics. Fig. 11, Fig. 12 and Fig. 13 depict the output voltage and current waveforms generated by three methods for the 5L, 7L and 7L configurations, respectively. The voltage harmonics exhibit values and percentages closely resembling those obtained with a purely resistive load. This underlines the negligible influence of load type and power factor on the output voltage waveform. Similar to Table 6, it is evident that in the majority of cases, SHE-PSO exhibits lower harmonic content compared to SBC and

Table 8. MLI output voltage and current THD with $R = 52.9\ \Omega$.

	Voltage Harmonic Content (V)								
	5L			7L			9L		
Maximum harmonic	SBC	SHE-PSO	SHE-NR	SBC	SHE-PSO	SHE-NR	SBC	SHE-PSO	SHE-NR
N_L	2.73	0.06	3.46	2.44	0.08	2.39	2.2	0.12	2.43
39th	16.15	16.00	17.06	10.91	11.17	10.64	7.85	10.50	7.72
49th	16.42	16.43	17.29	11.02	11.54	10.73	8.32	10.89	8.20
59th	16.64	16.56	17.42	11.31	11.61	11.01	8.38	11.02	8.28
Nyquist	17.58	17.46	18.35	12.2	12.51	11.89	9.33	11.67	9.20

Table 9. MLI output voltage harmonic content with $RL = 36\ \Omega - 0.153$ H.

	Voltage Harmonic Content (V)								
	5L			7L			9L		
Order	SBC	SHE-PSO	SHE-NR	SBC	SHE-PSO	SHE-NR	SBC	SHE-PSO	SHE-NR
1st	336.1 (100%)	339.8 (100%)	330.0 (100%)	330 (100%)	333.3 (100%)	334.7 (100%)	327 (100%)	329.9 (100%)	330.6 (100%)
3rd	6.9573 (2.07%)	0.2379 (0.07%)	11.5830 (3.51%)	4.9170 (1.49%)	0.3666 (0.11%)	0.2678 (0.08%)	3.5643 (1.09%)	0.4619 (0.14%)	0.4628 (0.14%)
5th	6.3523 (1.89%)	0.0680 (0.02%)	0.066 (0.02%)	0.3300 (0.10%)	0.0667 (0.02%)	0.0335 (0.01%)	1.3734 (0.42%)	0.0660 (0.02%)	0.0661 (0.02%)
7th				6.6990 (2.03%)	0.0000 (0.00%)	8.0328 (2.40%)	2.0928 (0.64%)	0.0330 (0.01%)	0.0661 (0.02%)
9th							6.0168 (1.84%)	0.0000 (0.00%)	8.0997 (2.45%)

Table 10. MLI output current harmonic content with $RL = 36\ \Omega - 0.153$ H.

	Current Harmonic Content (A)								
	5L			7L			9L		
Order	SBC	SHE-PSO	SHE-NR	SBC	SHE-PSO	SHE-NR	SBC	SHE-PSO	SHE-NR
1st	5.597 (100%)	5.657 (100%)	5.495 (100%)	5.495 (100%)	5.551 (100%)	4.683 (100%)	5.446 (100%)	5.494 (100%)	5.506 (100%)
3rd (0.84%)	0.0470 (0.03%)	0.0017 (1.42%)	0.0780 (0.60%)	0.0330 (0.04%)	0.0022 (0.04%)	0.0019 (0.44%)	0.0240 (0.06%)	0.0033 (0.06%)	0.0033
5th	0.0263 (0.47%)	0.0000 (0.00%)	0.0000 (0.00%)	0.0011 (0.02%)	0.0006 (0.01%)	0.0000 (0.00%)	0.0054 (0.10%)	0.0005 (0.01%)	0.0000 (0.00%)
7th				0.0198 (0.36%)	0.0000 (0.00%)	0.0234 (0.50%)	0.0060 (0.11%)	0.0000 (0.00%)	0.0000 (0.00%)
9th							0.0142 (0.26%)	0.0000 (0.00%)	0.0187 (0.34%)

SHE-NR. Once again, the 5th and 9th harmonic contents for SHE-NR stand out, particularly under 7L and 9L, as they are significantly higher than those of other methods at those orders.

In contrast, regarding current harmonics, it is apparent that overall, the current harmonics are significantly lower compared to the voltage harmonics, primarily due to the mentioned filtering effect. Generally, the SBC method yields an output current waveform with the highest harmonic contents. When comparing SHE-PSO and SHE-NR, both methods exhibit very low and similar harmonic contents from the 3rd harmonic order onwards. However, at the 7th harmonic for

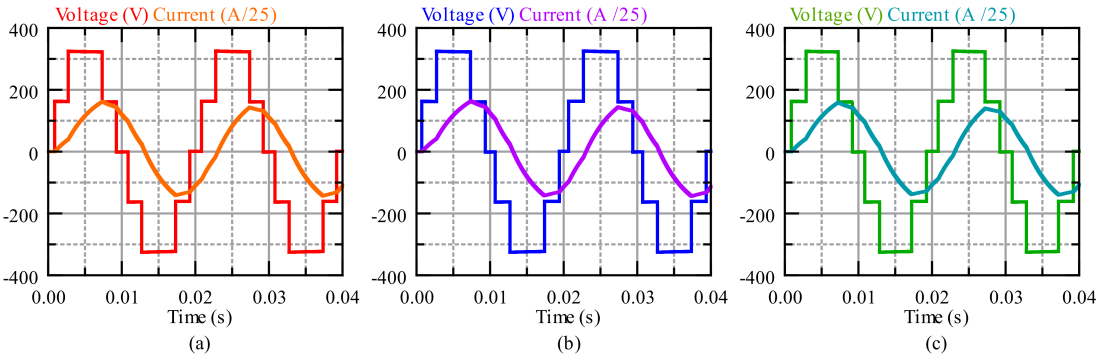

Figure 11. 5L output waveforms with $RL = 36\ \Omega - 0.153$ H generated by (a) SBC. (b) SHE-PSO. (c) SHE-NR.

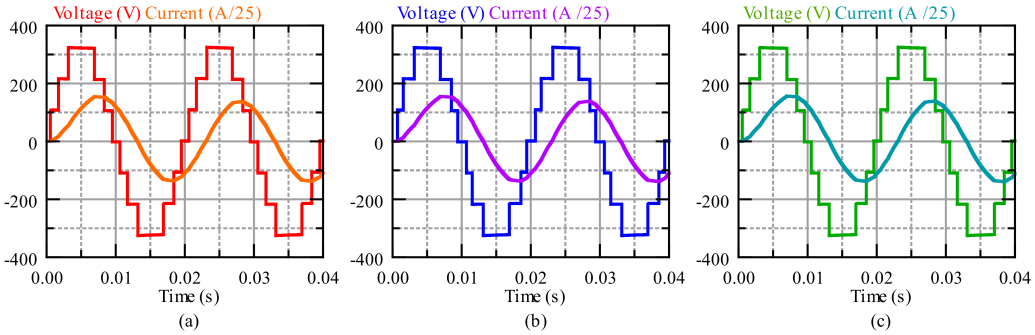

Figure 12. 7L output waveforms with $RL = 36\ \Omega - 0.153$ H generated by (a) SBC. (b) SHE-PSO. (c) SHE-NR.

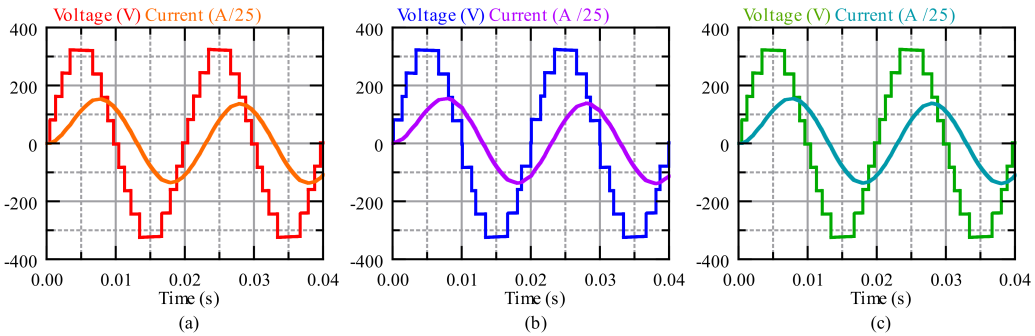

Figure 13. 9L output waveforms with $RL = 36\ \Omega - 0.153$ H generated by (a) SBC. (b) SHE-PSO. (c) SHE-NR.

the 5L MLI and at the 9th harmonic for the 9L MLI, SHE-NR displays considerably higher harmonic contents. Thus, the conclusion can be drawn that in terms of minimizing lower-order harmonics, SHE-PSO stands out as the most effective method.

Table 11 and Table 12 present the values of voltage THD and current THD, respectively obtained through the three techniques computed at various maximum harmonic orders under the tested RL load. The obtained THDs are also illustrated in Fig. 14 and Fig. 15. For the voltage THD, similar to the case of purely R load, in summary, SHE-PSO effectively reduces lower-order harmonics, yielding significantly

Table 11. MLI output voltage THD with $RL = 36\ \Omega - 0.153$ H.

	Voltage Harmonic Content (V)								
	5L			7L			9L		
Maximum harmonic	SBC	SHE-PSO	SHE-NR	SBC	SHE-PSO	SHE-NR	SBC	SHE-PSO	SHE-NR
N_L	2.80	0.07	3.51	2.52	0.11	2.40	2.27	0.14	2.45
39th	16.20	16.05	17.11	10.97	11.21	11.73	7.91	10.54	7.76
49th	16.47	16.48	17.34	11.08	11.59	10.78	8.38	10.93	8.25
59th	16.69	16.60	17.47	11.37	11.66	11.06	8.44	11.05	8.33
Nyquist	17.64	17.51	18.41	12.26	12.55	11.95	9.40	11.71	9.25

Table 12. MLI output current THD with $RL = 36\ \Omega - 0.153$ H.

	Current Harmonic Content (A)								
	5L			7L			9L		
Maximum harmonic	SBC	SHE-PSO	SHE-NR	SBC	SHE-PSO	SHE-NR	SBC	SHE-PSO	SHE-NR
N_L	0.96	0.03	1.42	0.70	0.04	0.50	0.53	0.06	0.34
39th	2.08	2.00	2.43	1.14	1.15	1.14	0.74	1.00	0.61
49th	2.08	2.00	2.43	1.14	1.15	1.15	0.74	1.01	0.61
59th	2.08	2.00	2.43	1.14	1.15	1.15	0.75	1.01	0.62
Nyquist	2.08	2.00	2.43	1.14	1.15	1.15	0.75	1.01	0.62

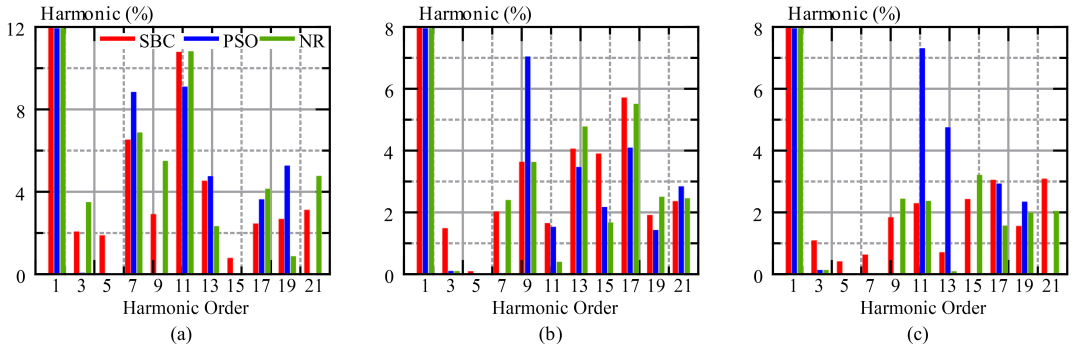

Figure 14. MLI output voltage harmonics with $RL = 36\ \Omega - 0.153$ H at (a) 5L. (b) 7L. (c) 9L.

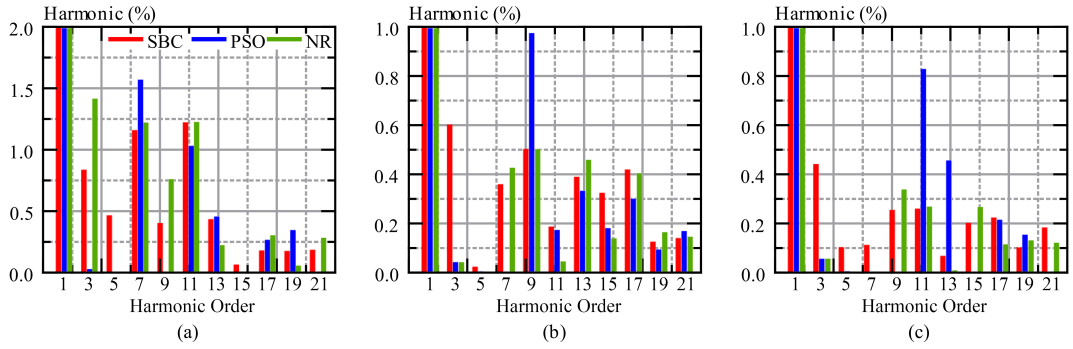

Figure 15. MLI output current harmonics with $RL = 36\ \Omega - 0.153$ H at (a) 5L. (b) 7L. (c) 9L.

lower THD when the maximum harmonic order is set at *NL*. However, at higher orders, eliminating lower harmonics doesn't consistently reduce overall THD. In the 5L MLI, SHE-PSO has the lowest overall THD, while for 7L and 9L MLIs, SHE-NR achieves the lowest THDs. As the number of levels increases, effectively reducing overall THD in MLIs becomes more challenging, and the importance of eliminating lower-order harmonics diminishes. As for the current THD, a similar trend is observed. Moreover, it is evident that current THDs, overall, are significantly lower than voltage THDs. This is attributed to effective waveform filtering, resulting in current waveforms closely resembling pure sinusoidal waveforms. In brief, regardless of the load type, only a general reduction in current harmonics is observed, which is not influenced by the optimization methods employed. Instead, it is primarily due to the filtering effects of the load's reactive components. Consequently, as with the *R* load case, minimizing lower-order harmonics does not guarantee a reduction in overall THD values.

4. Conclusion

Implementing MLI for switching signal generation becomes exceedingly complex as the number of levels increases, particularly when employing traditional modulation techniques like PWM. Consequently, researchers have increasingly turned to low-frequency pre-calculated switching angle methods in such scenarios. However, employing these switching methods tends to elevate output harmonics. Therefore, optimization techniques have been adopted to mitigate overall harmonics while still leveraging the practicality of low-frequency pre-calculated switching signal generation methods. This research aims to explore advanced optimization techniques for calculating switching angles in MLI systems, focusing on their viability and potential benefits, especially at higher levels. The goal is to evaluate if optimizing switching angles improves harmonic performance, processing power, and potential additional costs. Thus, this study assesses the application of PSO in solving SHE equations within multilevel inverter MLI systems, examining its impact on THD across different output levels. The investigation reveals that SHE-PSO successfully minimizes lower-order harmonics, surpassing simpler methods such as the SBC and SHE-NR. Despite this, the reduction in lower-order harmonics doesn't consistently translate to an overall enhancement in THD, especially at higher levels. Notably, at 5L, SHE-PSO demonstrates the lowest overall THD in comparison to SBC and SHE-NR. Conversely, at 7L and 9L, SHE-NR achieves the lowest THDs, with SHE-PSO exhibiting the highest values. This suggests that eliminating lower-order harmonics becomes less crucial for reducing overall THD as the number of levels increases. The study concludes that SHE-PSO effectively eliminates lower-order harmonics in MLIs, but the emphasis on reducing lower-order harmonics may not always lead to improved overall THD at higher MLI levels. Optimizing THD in high-level MLIs requires a more comprehensive exploration beyond the sole minimization of lower-order harmonics. In overall, the research contributes to understanding harmonic content optimization in MLIs, showcasing the efficacy of SHE-PSO for lower-order harmonic reduction while underscoring the complexities involved in achieving overall THD optimization at higher levels. Further research is imperative for the development of enhanced strategies aimed at

optimizing THD in high-level MLIs, ultimately leading to improved power quality and system efficiency.

Acknowledgment
The research work is financially supported by the Fundamental Research Grant Scheme (FRGS) from the Ministry of Higher Education Malaysia under Project FRGS/1/2024/TK08/USM/02/6.

Data Availability
This manuscript does not have associated data. All information and findings presented in this research are based on simulations, analyses, and theoretical considerations, and no specific datasets were generated or utilized for the purpose of this study. The results and conclusions drawn in this manuscript are solely derived from the methodologies described in the text.

Funding
FRGS/1/2024/TK08/USM/02/6.

Authors contributions
Authors have contributed equally in preparing and writing the manuscript.

Availability of data and materials
The data that support the findings of this study are available from the corresponding author upon reasonable request.

Conflict of interests
The authors declare that they have no known competing financial interests or personal relationships that could have appeared to influence the work reported in this paper.

References

[1] O. Ellabban and H. Abu-Rub. "**Z-Source Inverter: Topology Improvements Review**.". *IEEE Industrial Electronics Magazine*, 10 (1):6–24, 2016.
DOI: https://doi.org/10.1109/MIE.2015.2475475.

[2] M. Trabelsi, H. Vahedi, and H. Abu-Rub. "**Review on Single-DC-Source Multilevel Inverters: Topologies, Challenges, Industrial Applications, and Recommendations**.". *IEEE Open Journal of the Industrial Electronics Society*, 2:112–127, 2021.
DOI: https://doi.org/10.1109/OJIES.2021.3054666.

[3] R. A. Rana, S. A. Patel, A. Muthusamy, C. Woo Lee, and H.-J. Kim. "**Review of Multilevel Voltage Source Inverter Topologies and Analysis of Harmonics Distortions in FC-MLI**.". *Electronics*, 8 (11), 2019.
DOI: https://doi.org/10.3390/electronics8111329.

[4] F. K. Mohideen, N. A. M. Kajaan, Z. M. Isa, N. M. Nayan, M. H. Arshad, and S. S. Saad. "**THD analysis for symmetrical five level and seven level cascaded multilevel inverter**.". *J. Phys.: Conf. Ser.*, 1432(1):012020, 2020.
DOI: https://doi.org/10.1088/1742-6596/1432/1/012020.

[5] S. Shuvo, E. Hossain, T. Islam, A. Akib, S. Padmanaban, and Md. Z. R. Khan. "**Design and Hardware Implementation Considerations of Modified Multilevel Cascaded H-Bridge Inverter for Photovoltaic System**.". *IEEE Access*, 7:16504–16524, 2019.
DOI: https://doi.org/10.1109/ACCESS.2019.2894757.

[6] M. A. Hosseinzadeh, M. Sarebanzadeh, E. Babaei, M. Rivera, and P. Wheeler. "**A Switched-DC Source Sub-Module Multilevel Inverter Topology for Renewable Energy Source Applications**.". *IEEE Access*, 9:135964–135982, 2021.
DOI: https://doi.org/10.1109/ACCESS.2021.3115660.

[7] Y. Wang, J. Ye, R. Ku, Y. Shen, G. Li, and J. Liang. "**A modular switched-capacitor multilevel inverter featuring voltage gain ability**.". *J. Power Electron.*, 23(1):11–22, 2023.
DOI: https://doi.org/10.1007/s43236-022-00508-9.

[8] A. Vijayakumar, A. A. Stonier, G. Peter, A. K. Loganathan, and V. Ganji. "**Power quality enhancement in asymmetrical cascaded multilevel inverter using modified carrier level shifted pulse width modulation approach**.". *IET Power Electronics*.
DOI: https://doi.org/10.1049/pel2.12429.

[9] V. Kubendran, Y. Mohamed Shuaib, S. Vidyasagar, V. Kalyanasundaram, and K. Saravanan. "**The development of a generalized multilevel inverter for symmetrical and asymmetrical dc sources with a minimized ON state switch**.". *Ain Shams Engineering Journal*, 15(2):102358, 2024.
DOI: https://doi.org/10.1016/j.asej.2023.102358.

[10] F. L. Luo. "**Investigation on best switching angles to obtain lowest THD for multilevel DC/AC inverters**.". *IEEE 8th Conference on Industrial Electronics and Applications (ICIEA)*, page 1814–1818, 2013.
DOI: https://doi.org/10.1109/ICIEA.2013.6566663.

[11] S. T. Meraj, N. Z. Yahaya, K. Hasan, and A. Masaoud. "**A hybrid T-type (HT-type) multilevel inverter with reduced components**.". *Ain Shams Engineering Journal*, 12(2):1959–1971, 2021.
DOI: https://doi.org/10.1016/j.asej.2020.12.010.

[12] M. N. Hamidi, D. Ishak, M. A. A. M. Zainuri, and C. A. Ooi. "**Multilevel inverter with improved basic unit structure for symmetric and asymmetric source configuration**.". *IET Power Electronics*, 13(7):1445–1455, 2020.
DOI: https://doi.org/10.1049/iet-pel.2019.0916.

[13] A. Srivastava, A. Chauhan, and A. Tripathi. "**Design and performance evaluation of a novel modular asymmetrical multilevel inverter with minimal switches**.". *e-Prime - Advances in Electrical Engineering, Electronics and Energy*, 9:206–226, 2024.
DOI: https://doi.org/10.1016/j.prime.2024.100733.

[14] P. L. Kamani and M. A. Mulla. "**Middle-Level SHE Pulse-Amplitude Modulation for Cascaded Multilevel Inverters**.". *IEEE Transactions on Industrial Electronics*, 65(3):2828–2833, 2018.
DOI: https://doi.org/10.1109/TIE.2017.2742990.

[15] D. Gireesh Kumar et al. "**Design of an Optimized Asymmetric Multilevel Inverter with Reduced Components Using Newton-Raphson Method and Particle Swarm Optimization**.". *Mathematical Problems in Engineering*, page e9966708, 2023.
DOI: https://doi.org/10.1155/2023/9966708.

[16] M. Khizer, S. Liaquat, M. F. Zia, S. Kanukollu, A. Al-Durra, and S. M. Muyeen. "**Selective Harmonic Elimination in a Multilevel Inverter Using Multi-Criteria Search Enhanced Firefly Algorithm**.". *IEEE Access*, 11:3706–3716, 2023.
DOI: https://doi.org/10.1109/ACCESS.2023.3234918.

[17] M. Ali, F. S. Al-Ismail, M. M. Gulzar, and M. Khalid. "**A review on harmonic elimination and mitigation techniques in power converter based systems**.". *Electric Power Systems Research*, 234: 110573, 2024.
DOI: https://doi.org/10.1016/j.epsr.2024.110573.

[18] P. R. Bana, K. P. Panda, R. T. Naayagi, P. Siano, and G. Panda. "**Recently Developed Reduced Switch Multilevel Inverter for Renewable Energy Integration and Drives Application: Topologies, Comprehensive Analysis and Comparative Evaluation**.". *IEEE Access*, 7:54888–54909, 2019.
DOI: https://doi.org/10.1109/ACCESS.2019.2913447.

[19] D. Prasad, C. Dhanamjayulu, S. Padmanaban, J. B. Holm-Nielsen, F. Blaabjerg, and S. R. Khasim. "**Design and Implementation of 31-Level Asymmetrical Inverter With Reduced Components**.". *IEEE Access*, 9:22788–22803, 2021.
DOI: https://doi.org/10.1109/ACCESS.2021.3055368.

[20] M. He, M. Liu, R. Wang, X. Jiang, B. Liu, and H. Zhou. "**Particle swarm optimization with damping factor and cooperative mechanism**.". *Applied Soft Computing*, 76:45–52, 2019.
DOI: https://doi.org/10.1016/j.asoc.2018.11.050.

[21] C. Y. Hng, B. Ismail, M. Isa, and M. N. K. H. Rohani. "**Selective Harmonic Elimination Pulse Width Modulation for Five-Level Cascaded Inverter**.". *Journal of Telecommunication, Electronic and Computer Engineering (JTEC)*, 10(1-14):67–71, 2018.

[22] V. Padmathilagam and S. P. Natarajan. "**Solutions to the harmonic elimination problem in a seven level inverter**.". *International Journal of Power Electronics*, 1, 2009.
DOI: https://doi.org/10.1504/IJPELEC.2009.023623.

[23] W. A. Halim, T. N. A. T. Azam, K. Applasamy, and A. Jidin. "**Selective Harmonic Elimination Based on Newton-raphson Method for Cascaded H-bridge Multilevel Inverter**.". *International Journal of Power Electronics and Drive Systems (IJPEDS)*, 8 (3), 2017.
DOI: https://doi.org/10.11591/ijpeds.v8.i3.pp1193-1202.